Transverse Momentum and Centrality Dependence of High-p_T Nonphotonic Electron Suppression in Au + Au Collisions at $\sqrt{s_{NN}} = 200$ GeV

B. I. Abelev,[9] M. M. Aggarwal,[30] Z. Ahammed,[45] B. D. Anderson,[20] D. Arkhipkin,[13] G. S. Averichev,[12] Y. Bai,[28] J. Balewski,[17] O. Barannikova,[9] L. S. Barnby,[2] J. Baudot,[18] S. Baumgart,[50] V. V. Belaga,[12] A. Bellingeri-Laurikainen,[40] R. Bellwied,[48] F. Benedosso,[28] R. R. Betts,[9] S. Bhardwaj,[35] A. Bhasin,[19] A. K. Bhati,[30] H. Bichsel,[47] J. Bielcik,[50] J. Bielcikova,[50] L. C. Bland,[3] S-L. Blyth,[22] M. Bombara,[2] B. E. Bonner,[36] M. Botje,[28] J. Bouchet,[40] A. V. Brandin,[26] A. Bravar,[3] T. P. Burton,[2] M. Bystersky,[11] R. V. Cadman,[1] X. Z. Cai,[39] H. Caines,[50] M. Calderón de la Barca Sánchez,[6] J. Callner,[9] O. Catu,[50] D. Cebra,[6] Z. Chajecki,[29] P. Chaloupka,[11] S. Chattopadhyay,[45] H. F. Chen,[38] J. H. Chen,[39] J. Y. Chen,[49] J. Cheng,[43] M. Cherney,[10] A. Chikanian,[50] W. Christie,[3] S. U. Chung,[3] J. P. Coffin,[18] T. M. Cormier,[48] M. R. Cosentino,[37] J. G. Cramer,[47] H. J. Crawford,[5] D. Das,[45] S. Dash,[15] M. Daugherity,[42] M. M. de Moura,[37] T. G. Dedovich,[12] M. DePhillips,[3] A. A. Derevschikov,[32] L. Didenko,[3] T. Dietel,[14] P. Djawotho,[17] S. M. Dogra,[19] X. Dong,[22] J. L. Drachenberg,[41] J. E. Draper,[6] F. Du,[50] V. B. Dunin,[12] J. C. Dunlop,[3] M. R. Dutta Mazumdar,[45] V. Eckardt,[24] W. R. Edwards,[22] L. G. Efimov,[12] V. Emelianov,[26] J. Engelage,[5] G. Eppley,[36] B. Erazmus,[40] M. Estienne,[18] P. Fachini,[3] R. Fatemi,[23] J. Fedorisin,[12] A. Feng,[49] P. Filip,[13] E. Finch,[50] V. Fine,[3] Y. Fisyak,[3] J. Fu,[49] C. A. Gagliardi,[41] L. Gaillard,[2] M. S. Ganti,[45] E. Garcia-Solis,[9] V. Ghazikhanian,[7] P. Ghosh,[45] Y. G. Gorbunov,[10] H. Gos,[46] O. Grebenyuk,[28] D. Grosnick,[44] S. M. Guertin,[7] K. S. F. F. Guimaraes,[37] N. Gupta,[19] B. Haag,[6] T. J. Hallman,[3] A. Hamed,[41] J. W. Harris,[50] W. He,[17] M. Heinz,[50] T. W. Henry,[41] S. Heppelmann,[31] B. Hippolyte,[18] A. Hirsch,[33] E. Hjort,[22] A. M. Hoffman,[23] G. W. Hoffmann,[42] D. Hofman,[9] R. Hollis,[9] M. J. Horner,[22] H. Z. Huang,[7] E. W. Hughes,[4] T. J. Humanic,[29] G. Igo,[7] A. Iordanova,[9] P. Jacobs,[22] W. W. Jacobs,[17] P. Jakl,[11] F. Jia,[21] P. G. Jones,[2] E. G. Judd,[5] S. Kabana,[40] K. Kang,[43] J. Kapitan,[11] M. Kaplan,[8] D. Keane,[20] A. Kechechyan,[12] D. Kettler,[47] V. Yu. Khodyrev,[32] B. C. Kim,[34] J. Kiryluk,[22] A. Kisiel,[46] E. M. Kislov,[12] S. R. Klein,[22] A. G. Knospe,[50] A. Kocoloski,[23] D. D. Koetke,[44] T. Kollegger,[14] M. Kopytine,[20] L. Kotchenda,[26] V. Kouchpil,[11] K. L. Kowalik,[22] P. Kravtsov,[26] V. I. Kravtsov,[32] K. Krueger,[1] C. Kuhn,[18] A. I. Kulikov,[12] A. Kumar,[30] P. Kurnadi,[7] A. A. Kuznetsov,[12] M. A. C. Lamont,[50] J. M. Landgraf,[3] S. Lange,[14] S. LaPointe,[48] F. Laue,[3] J. Lauret,[3] A. Lebedev,[3] R. Lednicky,[13] C.-H. Lee,[34] S. Lehocka,[12] M. J. LeVine,[3] C. Li,[38] Q. Li,[48] Y. Li,[43] G. Lin,[50] X. Lin,[49] S. J. Lindenbaum,[27] M. A. Lisa,[29] F. Liu,[49] H. Liu,[38] J. Liu,[36] L. Liu,[49] T. Ljubicic,[3] W. J. Llope,[36] R. S. Longacre,[3] W. A. Love,[3] Y. Lu,[49] T. Ludlam,[3] D. Lynn,[3] G. L. Ma,[39] J. G. Ma,[7] Y. G. Ma,[39] D. Magestro,[29] D. P. Mahapatra,[15] R. Majka,[50] L. K. Mangotra,[19] R. Manweiler,[44] S. Margetis,[20] C. Markert,[42] L. Martin,[40] H. S. Matis,[22] Yu. A. Matulenko,[32] C. J. McClain,[1] T. S. McShane,[10] Yu. Melnick,[32] A. Meschanin,[32] J. Millane,[23] M. L. Miller,[23] N. G. Minaev,[32] S. Mioduszewski,[41] C. Mironov,[20] A. Mischke,[28] J. Mitchell,[36] B. Mohanty,[22] D. A. Morozov,[32] M. G. Munhoz,[37] B. K. Nandi,[16] C. Nattrass,[50] T. K. Nayak,[45] J. M. Nelson,[2] N. S. Nepali,[20] P. K. Netrakanti,[33] L. V. Nogach,[32] S. B. Nurushev,[32] G. Odyniec,[22] A. Ogawa,[3] V. Okorokov,[26] M. Oldenburg,[22] D. Olson,[22] M. Pachr,[11] S. K. Pal,[45] Y. Panebratsev,[12] A. I. Pavlinov,[48] T. Pawlak,[46] T. Peitzmann,[28] V. Perevoztchikov,[3] C. Perkins,[5] W. Peryt,[46] S. C. Phatak,[15] M. Planinic,[51] J. Pluta,[46] N. Poljak,[51] N. Porile,[33] A. M. Poskanzer,[22] M. Potekhin,[3] E. Potrebenikova,[12] B. V. K. S. Potukuchi,[19] D. Prindle,[47] C. Pruneau,[48] J. Putschke,[22] I. A. Qattan,[17] R. Raniwala,[35] S. Raniwala,[35] R. L. Ray,[42] D. Relyea,[4] A. Ridiger,[26] H. G. Ritter,[22] J. B. Roberts,[36] O. V. Rogachevskiy,[12] J. L. Romero,[6] A. Rose,[22] C. Roy,[40] L. Ruan,[22] M. J. Russcher,[28] R. Sahoo,[15] I. Sakrejda,[22] T. Sakuma,[23] S. Salur,[50] J. Sandweiss,[50] M. Sarsour,[41] P. S. Sazhin,[12] J. Schambach,[42] R. P. Scharenberg,[33] N. Schmitz,[24] J. Seger,[10] I. Selyuzhenkov,[48] P. Seyboth,[24] A. Shabetai,[18] E. Shahaliev,[12] M. Shao,[38] M. Sharma,[30] W. Q. Shen,[39] S. S. Shimanskiy,[12] E. P. Sichtermann,[22] F. Simon,[23] R. N. Singaraju,[45] N. Smirnov,[50] R. Snellings,[28] P. Sorensen,[3] J. Sowinski,[17] J. Speltz,[18] H. M. Spinka,[1] B. Srivastava,[33] A. Stadnik,[12] T. D. S. Stanislaus,[44] D. Staszak,[7] R. Stock,[14] M. Strikhanov,[26] B. Stringfellow,[33] A. A. P. Suaide,[37] M. C. Suarez,[9] N. L. Subba,[20] M. Sumbera,[11] X. M. Sun,[22] Z. Sun,[21] B. Surrow,[23] T. J. M. Symons,[22] A. Szanto de Toledo,[37] J. Takahashi,[37] A. H. Tang,[3] T. Tarnowsky,[33] J. H. Thomas,[22] A. R. Timmins,[2] S. Timoshenko,[26] M. Tokarev,[12] T. A. Trainor,[47] S. Trentalange,[7] R. E. Tribble,[41] O. D. Tsai,[7] J. Ulery,[33] T. Ullrich,[3] D. G. Underwood,[1] G. Van Buren,[3] N. van der Kolk,[28] M. van Leeuwen,[22] A. M. Vander Molen,[25] R. Varma,[16] I. M. Vasilevski,[13] A. N. Vasiliev,[32] R. Vernet,[18] S. E. Vigdor,[17] Y. P. Viyogi,[15] S. Vokal,[12] S. A. Voloshin,[48] W. T. Waggoner,[10] F. Wang,[33] G. Wang,[7] J. S. Wang,[21] X. L. Wang,[38] Y. Wang,[43] J. W. Watson,[20] J. C. Webb,[44] G. D. Westfall,[25] A. Wetzler,[22] C. Whitten, Jr.,[7] H. Wieman,[22] S. W. Wissink,[17] R. Witt,[50] J. Wu,[38] Y. Wu,[49] N. Xu,[22] Q. H. Xu,[22] Z. Xu,[3] P. Yepes,[36] I-K. Yoo,[34] Q. Yue,[43] V. I. Yurevich,[12] W. Zhan,[21] H. Zhang,[3] W. M. Zhang,[20] Y. Zhang,[38] Z. P. Zhang,[38] Y. Zhao,[38] C. Zhong,[39] J. Zhou,[36] R. Zoulkarneev,[13] Y. Zoulkarneeva,[13] A. N. Zubarev,[12] and J. X. Zuo[39]

(STAR Collaboration)

[1]*Argonne National Laboratory, Argonne, Illinois 60439, USA*
[2]*University of Birmingham, Birmingham, United Kingdom*
[3]*Brookhaven National Laboratory, Upton, New York 11973, USA*
[4]*California Institute of Technology, Pasadena, California 91125, USA*
[5]*University of California, Berkeley, California 94720, USA*
[6]*University of California, Davis, California 95616, USA*
[7]*University of California, Los Angeles, California 90095, USA*
[8]*Carnegie Mellon University, Pittsburgh, Pennsylvania 15213, USA*
[9]*University of Illinois, Chicago, Illinois 61801, USA*
[10]*Creighton University, Omaha, Nebraska 68178, USA*
[11]*Nuclear Physics Institute AS CR, 250 68 Řež/Prague, Czech Republic*
[12]*Laboratory for High Energy (JINR), Dubna, Russia*
[13]*Particle Physics Laboratory (JINR), Dubna, Russia*
[14]*University of Frankfurt, Frankfurt, Germany*
[15]*Institute of Physics, Bhubaneswar 751005, India*
[16]*Indian Institute of Technology, Mumbai, India*
[17]*Indiana University, Bloomington, Indiana 47408, USA*
[18]*Institut de Recherches Subatomiques, Strasbourg, France*
[19]*University of Jammu, Jammu 180001, India*
[20]*Kent State University, Kent, Ohio 44242, USA*
[21]*Institute of Modern Physics, Lanzhou, China*
[22]*Lawrence Berkeley National Laboratory, Berkeley, California 94720, USA*
[23]*Massachusetts Institute of Technology, Cambridge, Massachusetts 02139-4307, USA*
[24]*Max-Planck-Institut für Physik, Munich, Germany*
[25]*Michigan State University, East Lansing, Michigan 48824, USA*
[26]*Moscow Engineering Physics Institute, Moscow Russia*
[27]*City College of New York, New York City, New York 10031, USA*
[28]*NIKHEF and Utrecht University, Amsterdam, The Netherlands*
[29]*Ohio State University, Columbus, Ohio 43210, USA*
[30]*Panjab University, Chandigarh 160014, India*
[31]*Pennsylvania State University, University Park, Pennsylvania 16802, USA*
[32]*Institute of High Energy Physics, Protvino, Russia*
[33]*Purdue University, West Lafayette, Indiana 47907, USA*
[34]*Pusan National University, Pusan, Republic of Korea*
[35]*University of Rajasthan, Jaipur 302004, India*
[36]*Rice University, Houston, Texas 77251, USA*
[37]*Universidade de Sao Paulo, Sao Paulo, Brazil*
[38]*University of Science & Technology of China, Hefei 230026, China*
[39]*Shanghai Institute of Applied Physics, Shanghai 201800, China*
[40]*SUBATECH, Nantes, France*
[41]*Texas A&M University, College Station, Texas 77843, USA*
[42]*University of Texas, Austin, Texas 78712, USA*
[43]*Tsinghua University, Beijing 100084, China*
[44]*Valparaiso University, Valparaiso, Indiana 46383, USA*
[45]*Variable Energy Cyclotron Centre, Kolkata 700064, India*
[46]*Warsaw University of Technology, Warsaw, Poland*
[47]*University of Washington, Seattle, Washington 98195, USA*
[48]*Wayne State University, Detroit, Michigan 48201, USA*
[49]*Institute of Particle Physics, CCNU (HZNU), Wuhan 430079, China*
[50]*Yale University, New Haven, Connecticut 06520, USA*
[51]*University of Zagreb, Zagreb, HR-10002, Croatia*

(Received 11 July 2006; revised manuscript received 15 January 2007; published 10 May 2007)

The STAR collaboration at the BNL Relativistic Heavy-Ion Collider (RHIC) reports measurements of the inclusive yield of nonphotonic electrons, which arise dominantly from semileptonic decays of heavy flavor mesons, over a broad range of transverse momenta ($1.2 < p_T < 10$ GeV/c) in $p + p$, $d +$ Au, and Au + Au collisions at $\sqrt{s_{\mathrm{NN}}} = 200$ GeV. The nonphotonic electron yield exhibits an unexpectedly large suppression in central Au + Au collisions at high p_T, suggesting substantial heavy-quark energy loss at

RHIC. The centrality and p_T dependences of the suppression provide constraints on theoretical models of suppression.

DOI: 10.1103/PhysRevLett.98.192301 PACS numbers: 25.75.Dw, 13.20.Fc, 13.20.He, 13.85.Qk

High p_T hadron production measurements at the Relativistic Heavy-Ion Collider (RHIC) show a strong suppression of the single-particle inclusive yields in nuclear collisions [1–3]. The suppression is commonly thought to arise from partonic energy loss in dense matter due to induced gluon radiation [4], with its magnitude depending strongly on the color charge density of the medium. This makes it a sensitive probe of the matter created in heavy-ion collisions, where a quark-gluon plasma may form if sufficient energy density is achieved.

Charm and bottom quarks are produced dominantly through high-Q^2 partonic interactions. Heavy flavor cross sections and p_T spectra have been calculated at next-to-leading-order (NLO) for both $p + p$ and $A + A$ collisions [5–7], including nuclear matter effects [7]. Although pQCD calculations agree well with heavy-quark production in collider experiments at higher $\sqrt{s}$ [8], they disagree with recent RHIC measurements [9,10]. Nevertheless, measurements of heavy-quark production potentially provide new constraints on partonic energy loss mechanisms [11–17]. Gluon radiation in a forward cone is suppressed for heavy quarks at moderate energy (dead cone effect) [11,12], with corresponding reduction in medium induced energy loss and less suppression of heavy-quark mesons than light quark mesons.

Direct reconstruction of heavy flavor mesons via hadronic decay channels [9] is difficult in the complex environment of high energy nuclear collisions. Heavy-quark production can also be studied through measurements of electrons (positrons) from semileptonic D and B decays. This Letter reports STAR Collaboration measurements of the nonphotonic electron yield, $(e^+ + e^-)/2$, in $p + p$, $d + \mathrm{Au}$, and $\mathrm{Au} + \mathrm{Au}$ collisions at nucleon-nucleon center of mass energy $\sqrt{s_{\mathrm{NN}}} = 200$ GeV. The data extend significantly the p_T range of previous electron suppression studies [18], to a region of phase space where bottom decays are expected to be dominant. Large differences in energy loss are expected between c and b quarks in this region [14], and these measurements provide important new constraints on partonic energy loss mechanisms.

STAR is a large acceptance apparatus comprising several detector subsystems within a 0.5 T solenoidal magnet field [19]. The main detectors for this analysis are the Time Projection Chamber (TPC) [20] and the barrel Electromagnetic Calorimeter (EMC) [21]. The EMC has a gas-filled Shower Maximum Detector (SMD) at a depth of $\sim 5X_0$ to measure shower shape and position. A fast trigger based on single EMC tower energy enriches the electron sample at high p_T. Electrons at moderate p_T were reconstructed from minimum bias and centrality triggered $\mathrm{Au} + \mathrm{Au}$ event samples, while EMC triggered events were used for $p_T > 3 - 4\mathrm{GeV}/c$. $\mathrm{Au} + \mathrm{Au}$ data were divided into 3 centrality classes based on the track multiplicity measured at midrapidity. The integrated luminosity sampled by the EMC trigger is 100 nb^{-1} for $p + p$, 370 $\mu\mathrm{b}^{-1}$ for $d + \mathrm{Au}$ and 26 $\mu\mathrm{b}^{-1}$ for the most central $\mathrm{Au} + \mathrm{Au}$ events. The charged particle acceptance is $0 < \eta < 0.7$ and $0 < \phi < 2\pi$, selected to minimize the radiation length of detector material interior to the EMC within the available EMC acceptance.

The analysis has three main steps: selection of electrons, subtraction of background from decays and interactions in material, and residual corrections to the signal yield. Table I shows the major correction factors and uncertainties, which we now discuss in detail.

Electron PID.—Electron identification utilizes ionization energy loss (dE/dx) and track momentum from the TPC, together with energy and shower shapes from the EMC. Tracks with momentum $p > 1.5\mathrm{GeV}/c$ are accepted if they originate from the primary vertex (distance of closest approach less than 1.5 cm) and project to an active EMC tower, with acceptance $\alpha_{\mathrm{EMC}} \sim 75\%$–$85\%$ of the EMC instrumented coverage. This reduced acceptance is due to dead or noisy electronics channels. Initial electron identification is based on $p/E < 2$, where p is the TPC track momentum and E is the energy of the EMC tower. Simulations show that this cut excludes $\sim 7\%$ of real electrons due to sharing of shower energy between towers. Additional hadron rejection is based on the shower shape measured by the SMD. Figure 1(a) shows the dE/dx distribution for tracks passing the p/E and shower shape cuts. The curves show Gaussian functions fit to the distribution, representing the yields of $p + K$, pions and electrons [22]. The parameters in the fit are the yields, widths, and overall dE/dx scale, with widths and the distances between centroids being quasifree parameters, constrained by a model of energy deposition in the TPC gas [23].

Electrons are selected by cutting on TPC energy loss $dE/dx_{\mathrm{min}} < dE/dx < 5.1$ keV/cm. dE/dx_{min} is around 3.5 keV/cm, with the specific value having weak dependence on the event multiplicity and increasing slowly with track momentum, to optimize electron efficiency and hadron rejection while preserving more than 50% of the electrons in the dE/dx distribution. The residual hadron background satisfying the dE/dx cut is estimated based on Gaussian fits similar to those in Fig. 1.

Table I shows the combined electron tracking and identification efficiency (“PID efficiency”), determined by embedding simulated electrons into real events. It is significantly below unity due to tracking efficiency ($\sim 70\%$),

TABLE I. Corrections and systematic uncertainties for the nonphotonic electron yield at $p_T = 2$ and 8 GeV/c.

Correction	$p + p$		Central Au + Au	
	2 GeV/c	8 GeV/c	2 GeV/c	8 GeV/c
Acceptance	0.84 ± 0.05		0.75 ± 0.15	
PID efficiency	0.25 ± 0.03	0.50 ± 0.03	0.13 ± 0.03	0.45 ± 0.03
Hadron contamination	<0.01	0.20 ± 0.04	0.03 ± 0.03	0.22 ± 0.05
Background reconstruction efficiency (ε_B)	0.65 ± 0.06	0.55 ± 0.06	0.56 ± 0.06	0.50 ± 0.06
Bremsstrahlung & $\delta p/p$	0.86 ± 0.14	1.05 ± 0.05	0.9 ± 0.1	1.1 ± 0.1
EMC $\varepsilon_{\text{trigger}}$	-	1.00 ± 0.08	-	1.00 ± 0.05
Cross section	± 0.14		-	

exclusion of electrons due to the energy leakage to neighboring towers, and SMD response. Its increase from $p_T =$ 2 to 8 GeV/c is due to increasing SMD efficiency.

Electron background.—Background from photonic sources is due largely to photon conversions (~85%) in the detector material between the interaction point and the TPC ($X/X_0 \sim 4.5\%$) and π^0 and η Dalitz decays [24] (~15%). The photonic electron yield is measured using the invariant mass distribution of track pairs detected in the TPC. One track of the pair is required to fall in the EMC acceptance, satisfying $p > 1.5$ GeV/c and electron PID cuts, with the other track having $p_T > 0.15$ GeV/c within the TPC acceptance and a loose cut around the electron dE/dx band. Figure 1(b) shows the invariant mass distribution of pairs with the same or opposite charge sign. The same-sign distribution is due to random (combinatorial) pairs. An alternative combinatorial distribution formed by embedding single simulated electrons into real events agrees with the same-sign distribution within statistical uncertainties.

The shaded region in Fig. 1(b) is the difference between the opposite and same-sign distributions and represents the photonic yield. It exhibits a peak at zero invariant mass due to conversions, and a tail at nonzero mass due to Dalitz decays [24]. Selecting $m < 150$ MeV/c^2 accepts ~98% of all π^0 and η Dalitz pairs in this distribution. The efficiency $\varepsilon_B(p_T)$ to identify a photonic electron in the EMC by this procedure was estimated by embedding [25] the main background sources (π^0 and γ) with a realistic momentum distribution derived from recent RHIC data [26] into real events.

The photonic electron yield N_{ph} is calculated in each p_T bin via $N_{\text{ph}} = (N_{\text{unlike}} - N_{\text{like}})/\varepsilon_B$. Additional background, mainly from ω, ϕ, and ρ decays, was estimated using PYTHIA [27] and HIJING [28] simulations to be ~2%–4% of N_{ph} [9] and is included in the systematic uncertainty of N_{ph}. Figure 1(c) depicts the ratio of the inclusive to the photonic electron spectra for $p + p$ and Au + Au collisions. The figure shows a clear electron excess. Within uncertainties, the nonphotonic excess is independent of centrality at high p_T.

Nonphotonic electron yield.—The trigger efficiency was determined by comparing the electron candidate spectrum in the minimum bias and triggered data sets. At high-p_T the ratio of the spectra is compatible with the online scale-down factor applied to minimum bias events. The nonphotonic spectrum is the difference of the inclusive and photonic spectra. Additional corrections are applied for momentum resolution and bremsstrahlung, determined from simulations.

Systematic uncertainties.—Systematic uncertainties were determined by varying cut parameters within reasonable limits. The uncorrelated systematic uncertainty of the electron yield is dominated by the electron identification efficiency and photonic background reconstruction at low p_T and the correction for residual hadron background at high p_T.

Figure 2 shows the fully corrected nonphotonic electron spectra for 200 GeV $p + p$, $d +$ Au, and Au + Au collisions. The curves correspond to fixed order next-to-leading log (FONLL) predictions [7] for semileptonic D and B

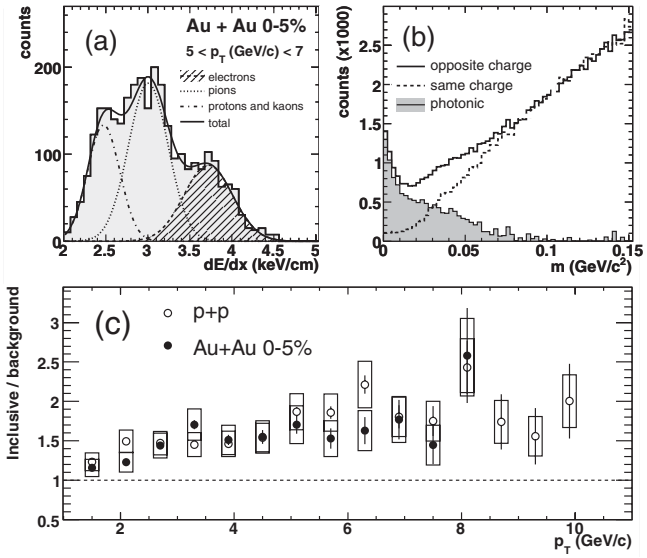

FIG. 1. (a) dE/dx projections for $5 < p_T(\text{GeV}/c) < 7$ in central Au + Au events after EMC and SMD cuts. The lines are Gaussian fits for $p + K$, π, and electron yields. (b) Invariant e^+e^- mass spectrum. (c) Ratio of inclusive and background electron yield vs p_T for $p + p$ and Au + Au collisions. Vertical bars are statistical errors, boxes are systematic uncertainties.

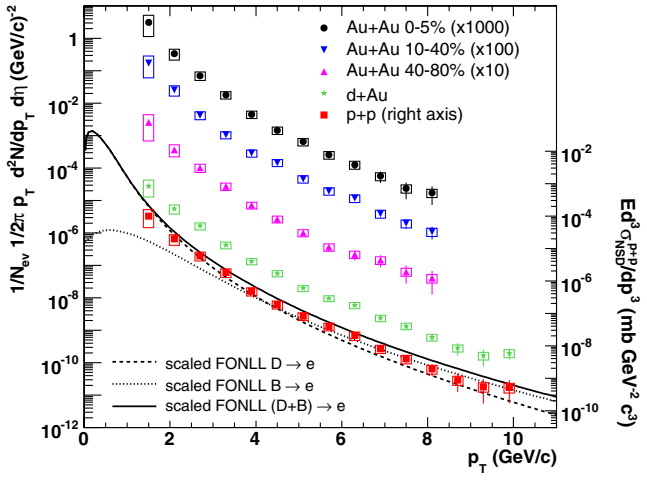

FIG. 2 (color online). Nonphotonic electron spectra. Vertical bars are statistical errors, boxes are systematic uncertainties. The curves are scaled pQCD predictions for $p + p$ [7]. Cross section on right axis applies to $p + p$ spectrum only.

meson decays. The calculated spectrum is scaled by 5.5 (see below).

Figure 3, upper part (points), shows the ratio of measured to unscaled FONLL-calculated nonphotonic electron yield for $p + p$ collisions. The calculation describes the *shape* of the measured spectra relatively well, though with a large difference in their overall scale. Better agreement is found at larger $\sqrt{s}$ [8]. The same ratio is shown for published STAR [9] and PHENIX [10] measurements. The horizontal dashed line is at $5.5 \pm 0.8(\text{stat}) \pm 1.7(\text{syst})$, corresponding to the ratio between the total charm cross section measured by STAR [9] to the central value predicted by FONLL [7,8]. The shaded band around that line shows the experimental uncertainty in this ratio. PHENIX data [10] exhibit a lower ratio and appear not to be consistent with the data reported here. The lower part (curves) shows the relative contribution to the FONLL calculation of charm and bottom decays, with the variation due to NLO uncertainties [7,29]. The B-decay contribution is expected to be significant in the upper p_T range of this measurement.

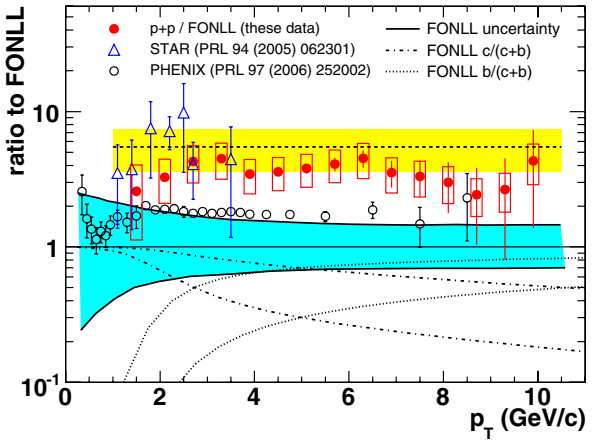

FIG. 3 (color online). Upper: ratio between measured nonphotonic electron yield and FONLL pQCD calculations [7] for $p + p$ collisions. Lower: relative contributions to FONLL distribution of c and b decays.

Modification of the inclusive particle production is measured by the nuclear modification factor [1] [$R_{AA}(p_T)$]. R_{AA} is unity for hard processes without nuclear effects. Figure 4 shows $R_{AA}(p_T)$ for nonphotonic electrons in d + Au and central Au + Au collisions. Error bars show the statistical uncertainties, boxes show uncorrelated systematic uncertainties, and the filled band at unity is the overall normalization uncertainty. R_{AA} for d + Au is consistent with a moderate Cronin enhancement. $R_{AA} \sim 0.2$ for central Au + Au collisions at $p_T > 3$ GeV/c, consistent with a previous measurement at lower p_T [18]. The suppression is similar to that for light hadrons at $p_T > 6$ GeV/c [2].

Figure 4 shows predictions for electron R_{AA} from semileptonic D- and B-meson decay in central Au + Au collisions using calculations of heavy-quark energy loss. Curve I uses DGLV radiative energy loss via few hard scatterings [14] with initial gluon density $dN_g/dy = 1000$, consistent with light quark suppression. Curve II uses BDMPS radiative energy loss via multiple soft collisions [15], with transport coefficient $\hat{q}$. $\hat{q}$ is set to 14 GeV^2/fm, though light quark hadron suppression provides only a loose constraint $4 < \hat{q} < 14$ GeV^2/fm [15]. Both calculations predict much less suppression than observed.

This discrepancy may indicate significant collisional (elastic) energy loss for heavy quarks [13,30]. Curve III is a DGLV-based calculation including both radiative *and* collisional energy loss, together with path length fluctua-

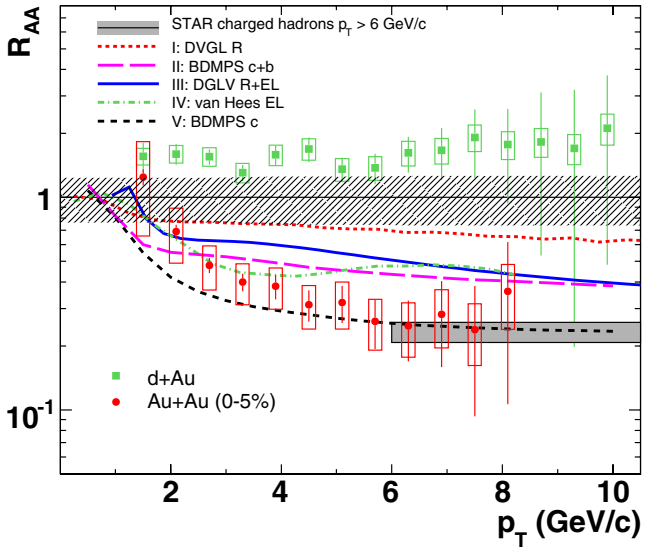

FIG. 4 (color online). The nuclear modification factor, R_{AA}, for d + Au and Au + Au collisions at $\sqrt{s_{NN}} = 200$ GeV. Error bars and uncertainties are described in text.

tions [16]. The calculated suppression is also markedly less than that observed. For curve IV, the heavy-quark energy loss is due to elastic scattering mediated by resonance excitations (D and B) and LO t-channel gluon exchange [17]. This calculation also predicts significantly less suppression than observed.

Dead cone reduction of energy loss is expected to be more significant for bottom than charm quarks in the reported p_T range. Curve V, which is the same calculation as curve II but for D-meson decays only, agrees better with the data. Since there is better agreement of data and theory for bottom than charm production at the Tevatron [8], the scale factor 5.5 between calculated and measured $p + p$ electron yields may overestimate the B decay contribution at RHIC; i.e., D decays may in fact dominate the electron yields in the reported p_T range, favoring calculation V. A direct measurement of D mesons at high-p_T is required to understand energy loss of heavy quarks in detail. Finally, multibody mechanisms may also contribute to heavy-quark energy loss [31].

We have reported the measurement of high-p_T nonphotonic electrons in $p + p$, $d + \mathrm{Au}$, and $\mathrm{Au} + \mathrm{Au}$ collisions at $\sqrt{s_{\mathrm{NN}}} = 200$ GeV. A pQCD calculation for heavy-quark production in $p + p$ collisions underpredicts the data, although it describes the overall shape of the p_T distribution relatively well. Large yield suppression is observed in central $\mathrm{Au} + \mathrm{Au}$ collisions, consistent with substantial energy loss of heavy quarks in dense matter. The suppression is larger than that expected from radiative energy loss calculations, suggesting that other processes contribute significantly to heavy-quark energy loss. This unique sensitivity to the energy loss mechanisms makes the measurement of heavy-quark suppression an essential component of the study of dense matter. Full description of the interaction between partons and the medium will require further detailed measurements of charm and bottom separately.

We thank the RHIC Operations Group and RCF at BNL, and the NERSC Center at LBNL for their support. This work was supported in part by the HENP Divisions of the Office of Science of the U. S. DOE; the U. S. NSF; the BMBF of Germany; IN2P3, RA, RPL, and EMN of France; EPSRC of the United Kingdom; FAPESP of Brazil; the Russian Ministry of Science and Technology; the Ministry of Education and the NNSFC of China; IRP and GA of the Czech Republic, FOM of the Netherlands, DAE, DST, and CSIR of the Government of India; Swiss NSF; the Polish State Committee for Scientific Research; STAA of Slovakia, and the Korea Sci. & Eng. Foundation.

[1] C. Adler *et al.*, Phys. Rev. Lett. **89**, 202301 (2002).
[2] J. Adams *et al.*, Phys. Rev. Lett. **91**, 172302 (2003).
[3] J. Adams *et al.*, Phys. Rev. Lett. **91**, 072304 (2003).
[4] R. Baier *et al.*, Annu. Rev. Nucl. Part. Sci. **50**, 37 (2000); M. Gyulassy *et al.*, arXiv:nucl-th/0302077.
[5] S. Frixione *et al.*, Adv. Ser. Dir. High Energy Phys. **15**, 609 (1998).
[6] R. Vogt, Heavy Ion Physics **18**, 11 (2003).
[7] M. Cacciari *et al.*, Phys. Rev. Lett. **95**, 122001 (2005); FONLL calculations with CTEQ6M, $m_c = 1.5\ \mathrm{GeV}/c^2$, $m_b = 5\ \mathrm{GeV}/c^2$, and $\mu_{R,F} = m_T$.
[8] S. Frixione, Eur. Phys. J. C **43**, 103 (2005).
[9] J. Adams *et al.*, Phys. Rev. Lett. **94**, 062301 (2005).
[10] A. Adare *et al.*, Phys. Rev. Lett. **97**, 252002 (2006).
[11] Yu. L. Dokshitzer and D. E. Kharzeev, Phys. Lett. B **519**, 199 (2001).
[12] B. W. Zhang *et al.*, Phys. Rev. Lett. **93**, 072301 (2004).
[13] M. G. Mustafa, Phys. Rev. C **72**, 014905 (2005).
[14] M. Djordjevic *et al.*, Phys. Lett. B **632**, 81 (2006).
[15] N. Armesto *et al.*, Phys. Lett. B **637**, 362 (2006).
[16] S. Wicks *et al.*, Nucl. Phys. **A784**, 426 (2007).
[17] H. van Hees, V. Greco, and R. Rapp, Phys. Rev. C **73**, 034913 (2006); (private comunication).
[18] S. S. Adler *et al.*, Phys. Rev. Lett. **96**, 032301 (2006).
[19] K. H. Ackermann *et al.*, Nucl. Instrum. Methods Phys. Res., Sect. A **499**, 624 (2003).
[20] M. Anderson *et al.*, Nucl. Instrum. Methods Phys. Res., Sect. A **499**, 659 (2003).
[21] M. Beddo *et al.*, Nucl. Instrum. Methods Phys. Res., Sect. A **499**, 725 (2003).
[22] M. Shao *et al.*, Nucl. Instrum. Methods Phys. Res., Sect. A **558**, 419 (2006).
[23] H. Bichsel, Nucl. Instrum. Methods Phys. Res., Sect. B **562**, 154 (2006).
[24] S. Eidelman *et al.*, Phys. Lett. B **592**, 1 (2004).
[25] J. Adams *et al.*, arXiv:nucl-ex/0311017.
[26] S. S. Adler *et al.*, Phys. Rev. Lett. **98**, 172302 (2007).
[27] T. Sjostrand *et al.*, arXiv:hep-ph/0308153.
[28] M. Gyulassy and X. N. Wang, Comput. Phys. Commun. **83**, 307 (1994).
[29] R. Vogt (private communication).
[30] M. Djordjevic, Phys. Rev. C **74**, 064907 (2006).
[31] W. Liu and C. M. Ko, arXiv:nucl-th/0603004.